

Improved Solid-State Photomechanical Materials by Fluorine Substitution of 9-Anthracene Carboxylic Acid

Lingyan Zhu,[†] Fei Tong,[†] Christopher Salinas,[‡] Muhanna K. Al-Muhanna,[§] Fook S. Tham,[†] David Kisailus,^{‡,||} Rabih O. Al-Kaysi,^{*,†,⊥} and Christopher J. Bardeen^{*,†}

[†]Department of Chemistry, University of California, Riverside, 501 Big Springs Road, Riverside, California 92521, United States

[‡]Department of Chemical and Environmental Engineering, University of California, Riverside, 900 University Avenue, Riverside, California 92521, United States

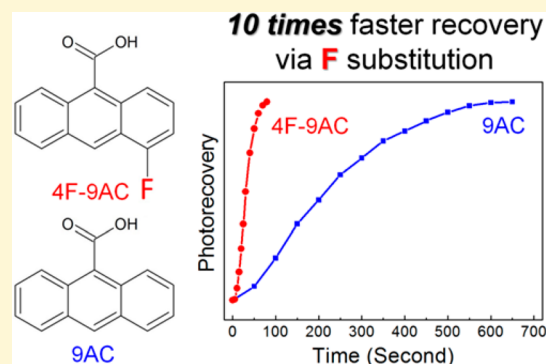
[§]King Abdulaziz City for Science and Technology, P.O Box 6086, Riyadh 11442, Kingdom of Saudi Arabia

^{||}Materials Science and Engineering Program University of California, Riverside, 900 University Avenue, Riverside, California 92521, United States

[⊥]Department of Basic Science, College of Science and Health Professions-3124, King Saud bin Abdulaziz University for Health Sciences, and King Abdullah International Medical Research Center, Ministry of National Guard Health Affairs, Riyadh 11426, Kingdom of Saudi Arabia

Supporting Information

ABSTRACT: Four fluorinated derivatives of 9-anthracene carboxylic acid (9AC), a molecule that shows a reversible photomechanical response in its crystal form, have been synthesized and characterized. The spectroscopic properties and crystal structures of 4-fluoro-9-anthracene carboxylic acid (4F-9AC), 2-fluoro-9-anthracene carboxylic acid (2F-9AC), 10-fluoro-9-anthracene carboxylic acid (10F-9AC), and 2,6-difluoro-9-anthracene carboxylic acid (2,6DF-9AC) are all very similar to those of 9AC. However, their photomechanical properties vary widely. 405 nm light was used to induce [4 + 4] photodimerization and a mechanical response in crystalline microneedles and ribbons. Both the photodimer dissociation rate and the mechanical recovery varied by more than an order of magnitude, with 4F-9AC exhibiting the most rapid recovery time, on the order of 30 s. Nanoindentation measurements show that this crystal has a slightly reduced elastic modulus and a significantly reduced hardness, making it less brittle than the 9AC crystal. Large 4F-9AC crystals remain intact after irradiation, without fragmenting, while microneedles can undergo more than 100 mechanical bending cycles. Given the similarity of the crystal packing in all five molecules, the improved photomechanical properties must arise from subtle changes in intermolecular interactions or possibly differences in disorder. These results demonstrate that it is possible to significantly improve the properties of photomechanical materials through small modifications of the molecular structure.



INTRODUCTION

Photons can be transformed into mechanical motion by photochemical reactions in which molecules change shape or bonding configuration. If photochemically reactive molecules are organized, for example in a molecular crystal or a liquid crystalline polymer, then each photochemical reaction can “push” in the same direction. The sum of many such displacements, on the angstrom scale, can result in a large total displacement on the scale of micrometers or more. This is the origin of photomechanical effects in molecular materials.¹ Such materials have potential applications as photocontrolled actuators and as elements of photon-fueled machines. Photomechanical materials where the photoreactive molecule is embedded in a polymer host have been developed and have demonstrated interesting photomechanical properties.^{2–4} Neat molecular crystals, composed solely of photoreactive molecules

without a host, can also function as photomechanical materials and have several potential advantages.^{5–11} From a mechanistic standpoint, the structure of molecular crystals can be precisely characterized using X-ray diffraction, making it possible to study in detail how reaction dynamics lead to crystal deformation. Molecular crystals tend to have higher elastic moduli than polymers.¹² Irie and co-workers have shown that the photomechanical response of diarylethene crystals can be very fast and persist even at very low temperatures.^{13–15}

In order to use a molecular crystal as a reversible photoactuator, the underlying photochemistry must be reversible. For example, the ring closing reaction of diary-

Received: August 4, 2014

Revised: September 10, 2014

lethene photochromes can be initiated by ultraviolet light, while the reverse reaction requires illumination at visible wavelengths to return the ring to its open form.¹⁶ The use of a single light source to induce repeated deformations simplifies the operation of such actuators but requires a photoreaction that can be reversed by ambient thermal fluctuations. One such reaction is the [4 + 4] photodimerization of crystalline 9-anthracene carboxylic acid (**9AC**), which generates a metastable head-to-head dimer that spontaneously dissociates to the monomer pair at room temperature.¹⁷ This reaction formed the basis of molecular crystal nanorods and microribbons that could reversibly bend and twist in response to a pulse of monochromatic light.^{18–20} As a practical photoactuator material, however, **9AC** has several drawbacks. First, this molecule is not particularly photostable, perhaps due to endoperoxidation reactions with ambient O₂, and typically a crystal can only undergo 10 cycles before a significant amount of response is lost.¹⁸ Second, the slow dimer dissociation time (~400 s) means that the duty cycle of an actuator based on this molecule will be low. Third, **9AC** crystals are relatively brittle, and crystals with thicknesses greater than about 10 μm tend to crack or shatter under illumination. We and others have shown that the use of nanoscale crystals provides a general solution to the problem of fragmentation,^{21–23} but it is desirable to find a material which has a useful photomechanical response over a larger size range. To circumvent these problems, we recently explored a family of **9AC** derivatives with substituents at the 10-position, opposite the COOH group.²⁴ While none of those derivatives improved upon the performance of **9AC**, 10-fluoro-9-anthracene carboxylic acid (**10F-9AC**) did exhibit a reversible photomechanical response, albeit much slower than **9AC**.

In this paper, we continue our pursuit of improved derivatives of **9AC**. We have concentrated our efforts on fluoro-substituted derivatives, since this atom is close in size to hydrogen and should minimize size-induced disruptions of the crystal lattice. At the same time, the presence of electron-withdrawing groups should lower the HOMO and LUMO levels, increasing the stability of the molecule with respect to oxidative side reactions.²⁵ The goal of the research is to identify molecules that have (a) a faster dissociation and mechanical recovery rate and (b) greater photostability. With this in mind, we undertook a comparative study of the **9AC** derivatives shown in Figure 1. We have previously reported results on **9AC** and **10F-9AC** but the other three molecules, 4-fluoro-9-anthracene carboxylic acid (**4F-9AC**), 2-fluoro-9-anthracene carboxylic acid (**2F-9AC**), and 2,6-difluoro-9-anthracene carboxylic acid (**2,6DF-9AC**), are newly synthesized derivatives. For completeness, in this paper we consider all five molecules as a group. We find that the spectroscopic properties of the molecules in both solution and solid-state are very similar. The behaviors of these molecules diverge strongly when their photomechanical properties are considered, however. The most promising molecule, **4F-9AC**, has a back-reaction rate that is almost 1 order of magnitude faster than that of **9AC**, as well as higher photostability with the ability to undergo >100 photomechanical cycles without loss of function. Using nanoindentation measurements, we find that crystals composed of **4F-9AC** have a similar elastic modulus to **9AC**, but are a factor of 2 less hard. This decreased hardness allows larger **4F-9AC** crystals to remain intact while they undergo photomechanical deformations. **4F-9AC** retains the properties of **9AC** that make it a photomechanical material (head-to-head crystal packing mediated by hydrogen-bonding interactions)

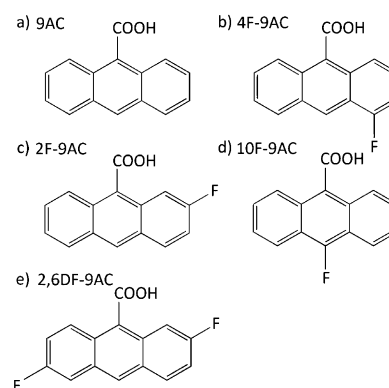


Figure 1. Molecular structures of anthracene-9-carboxylic acid (**9AC**) and its fluorinated derivatives: (a) anthracene-9-carboxylic acid (**9AC**); (b) 4-fluoro-anthracene-9-carboxylic acid (**4F-9AC**); (c) 2-fluoro-anthracene-9-carboxylic acid (**2F-9AC**); (d) 10-fluoro-anthracene-9-carboxylic acid (**10F-9AC**); and (e) 2,6-difluoro-anthracene-9-carboxylic acid (**2,6DF-9AC**).

but is significantly superior to **9AC** in terms of properties that would be desired for a practical photoactuator. The results of this paper show that it is possible to systematically vary the molecular structure to improve the solid-state photomechanical properties.

EXPERIMENTAL SECTION

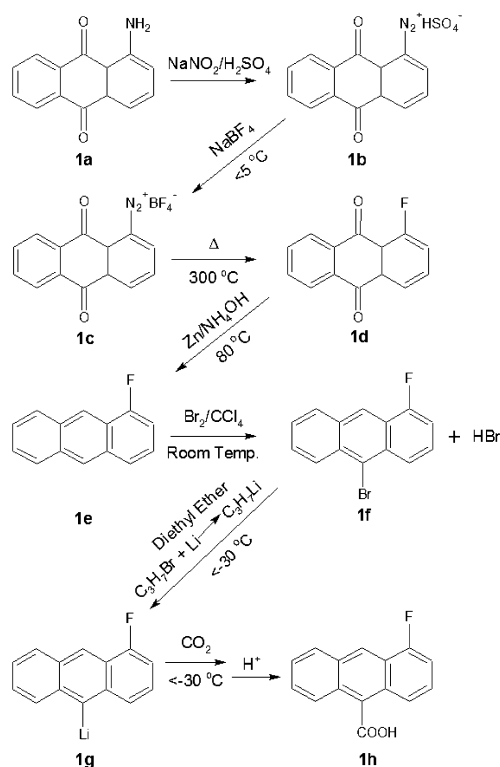
Synthesis of Fluoro-9-anthracene Carboxylic Acid Derivatives. All starting materials were purchased from the Tokyo Chemical Industry Company (TCI) and used without further purification. Dry diethyl ether was distilled over lithium aluminum hydride and stored over activated molecular sieves (4 Å). All other organic solvents were distilled over anhydrous CaCl₂ prior to use. Glassware was kept dry in an oven at 60 °C prior to use. Melting points (uncorrected) were measured on a 1101D Mel-Temp digital melting point apparatus. IR measurements were performed using IR Affinity-1 FTIR from Shimadzu. GC-MS data were collected using Shimadzu GCMS-QP2010 using a 30 m long general-purpose capillary GC column.

4-Fluoro-9-anthracene Carboxylic Acid (4F-9AC). The detailed synthesis of **4F-9AC** is depicted in Scheme 1. The syntheses of the other fluoro-9-anthracene carboxylic acid derivatives are similar and are described in the Supporting Information.

1-Antraquinone Diazonium Tetrafluoroborate 1c.²⁶ In a 250 mL Erlenmeyer flask, 1-aminoanthraquinone **1a** (3 g, 0.013 mol) was dissolved in 98% H₂SO₄ (50 mL) at room temperature to give a dark brown solution. NaNO₂ (2.5 g, 0.036 mol), previously dissolved in ice-cold 98% H₂SO₄ (25 mL), was added slowly to **1a** in H₂SO₄ at 0 °C. The temperature was kept at <5 °C throughout the addition process, which took 10–15 min. The reaction mixture was stirred at <5 °C for 1 h before pouring the contents over 400 mL of crushed ice. 1-Antraquinone diazonium hydrogen sulfate **1b** precipitated out as a sparingly soluble pink solid. To the aqueous suspension of **1b**, NaBF₄ (3 g, 0.028 mol) was added and stirred at 0 °C for 2 h to precipitate out the insoluble tetrafluoroborate salt **1c**. The pinkish solid was filtered over crushed ice and then washed with ice-cold water (50 mL) followed by cold ethanol (10 mL). The powder was rinsed with hexane (20 mL) before leaving it to air-dry at room temperature for several hours. We obtained **1c** as a white pink powder (3.6 g, 84% yield).

1-Fluoro-anthraquinone 1d. Compound **1c** (3.6 g, 0.011 mol) was mixed with six times its weight in sand (20 g), placed on a 25 cm × 25 cm piece of aluminum foil, and folded into a flat puck-shaped disk. The disk was placed flat inside a 500 mL beaker and decomposed at 300 °C for 24 h. The beaker was covered with aluminum foil to collect the sublimed **1d** as large red needle-like crystals (2.0 g, 78% yield) with a mp of 230–231 °C (literature mp: 230–232 °C²⁷). The

Scheme 1. Synthetic Scheme for Compound 4-Fluoro-9-anthracene Carboxylic Acid (4F-9AC)



crystals can be easily separated from the decomposed byproducts that formed a black solid lump with the sand inside the aluminum foil. GC-MS revealed that the product was 95% **1d** with $M^+ = 226$ corresponding to the molecular ion peak and fragments at 198 (loss of one CO) and 170 (loss of two CO).

1-Fluoroanthracene 1e. Compound **1d** (2.0 g, 0.0088 mol) was suspended with 27% ammonium hydroxide solution (50 mL), water (50 mL), and CuSO_4 (0.05 g) in a 500 mL round-bottom flask. Zn powder (4 g, 0.0625 g), prewashed with acid, was added to the mixture and stirred vigorously at 80°C . The round-bottom flask was fitted with a six segment Snyder column that allows excess ammonia gas to escape while stopping air from flowing back inside the flask. The reaction changes from deep red to a turbid white after 24 to 36 h when all of the **1d** is reduced to the corresponding anthracene **1e**. The suspension of **1e** and $\text{Zn}(\text{OH})_2$ was filtered and stirred with HCl (200 mL, 2 M) to dissolve the $\text{Zn}(\text{OH})_2$. The undissolved **1e** was suction filtered and washed with water before recrystallizing from boiling 1-propanol (30 mL) and water (30 mL). We obtained pale green platelike crystals of **1e** (0.81 g, 47% yield) with a mp of $108\text{--}109^\circ\text{C}$ (literature mp: 108°C ^{28,29}). $^1\text{H NMR}$ (CDCl_3) δ (ppm): 7.32 (1H, t), 7.35 (1H, m), 7.40 (1H, d), 7.48 (1H, d), 7.51 (1H, m), 7.77–8.00 (2H, dd), 8.4 (1H, s), 8.6 (1H, s). GC-MS demonstrated 98% **1e** with a major peak corresponding to $M^+ = 196$ and minor fragment at 170.

9-Bromo-4-fluoroanthracene 1f. Compound **1e** (0.80 g, 0.0041 mol), previously dried under vacuum, was dissolved in warm CCl_4 (30 mL). Bromine liquid (0.72 g, 0.23 mL, 1.1 equiv) was added slowly and allowed to react at room temperature overnight. The mixture was filtered through silica gel (10 g, flash chromatography grade) then eluted with 200 mL of hexane. The organic solvent was removed under reduced pressure to yield yellow crystals of **1f** (0.82 g, 72% yield) with a mp of $99\text{--}101^\circ\text{C}$. $^1\text{H NMR}$ (CDCl_3) δ (ppm): 7.16 (1H, t), 7.49 (2H, m), 7.55 (1H, dd), 8.04 (1H, d), 8.30 (1H, d), 8.48 (1H, d), 8.71 (1H, s). GC-MS showed a very pure product with two equal intensity peaks at $M^+ = 276$ and 274, corresponding to a monobrominated product and fragment peaks at 196 and 194 corresponding to loss of one bromine. The powder was dried under

vacuum (200 mbar) at 90°C for several hours to remove any trace of water in preparation for the lithiation step.

4-Fluoro-9-anthracene Carboxylic Acid (4F-9AC). In a 50 mL oven-dried round-bottom flask, dry diethyl ether (10 mL) was added to 1-bromopropane (0.54 g, 0.4 mL, 0.0044 mol). Freshly cut lithium wire (0.18 g, 0.03 mol) was flattened and then stirred with the 1-bromopropane in diethyl ether under an argon atmosphere to prepare *n*-propyllithium. Unreacted lithium was fished out and reweighed to confirm conversion of most of the 1-bromopropane to its lithium salt. The *n*-propyllithium/diethyl ether solution was cooled to -30°C using Lab Armor dry bath beads before adding **1f** (0.2 g, 7.3×10^{-4} moles) and stirring for 20 min to produce **1g**. While maintaining the temperature at -30°C , CO_2 gas was bubbled through the mixture for 20 min using two 1 L balloons inflated with dry CO_2 . The reaction was quenched by adding it to crushed ice (50 mL) followed by extracting the insoluble organic residue with ethyl acetate (50 mL) followed by hexanes (2×50 mL). The acid was precipitated out of the aqueous solution by adding concentrated HCl (3 mL). The yellow precipitate was suction filtered and recrystallized from boiling ethanol (10 mL) and water (10 mL). We obtained a yellow powder of **1h** (0.13 g, 77% yield) with a mp of $257\text{--}258^\circ\text{C}$. $^1\text{H NMR}$ (CDCl_3) δ (ppm): 7.37 (1H, dd), 7.61 (3H, m), 7.84 (1H, d), 8.03 (1H, d), 8.26 (1H, d), 8.86 (1H, s). ν_{max} (KBr disc) cm^{-1} : 3500–2800 (broad, COOH), 1682 (CO), 1639 (C=C), 1559, 1457, 1278, 1249, 720.

X-ray Structure Determination. Crystals of the other fluoro-9-anthracene carboxylic acids were prepared by subliming a sample under normal atmospheric pressure at 180°C . They were mounted on a cryo-loop glass fiber with paratone oil. Single-crystal X-ray diffraction data were collected on a Bruker APEX2 platform-CCD X-ray diffractometer system (fine focus Mo radiation, $\lambda = 0.71073 \text{ \AA}$, 50KV/35 mA power) at 100 K. The frames were collected for a sphere of reflections and integrated using the Bruker SAINT software package and using a narrow-frame integration algorithm. Absorption corrections were applied to the raw intensity data using the SADABS program. The Bruker SHELXTL software package was used for phase determination and structure refinement. The **4F-9AC**, **10F-9AC**, and **2,6DF-9AC** crystals were all found to be twinned structures. The **2F-9AC** crystal included about 20% of a 2-fluoro-anthracene byproduct, likely the result of decomposition during the sublimation process. The **10F-9AC** crystal had about 5% of a residual 10-bromo-9-anthracene carboxylic byproduct left over from the synthesis. Both **4F-9AC** and **2,6DF-9AC** had significant disorder in the fluorine positions due to different orientations of the anthracene in the stack. All these complications were taken into account in the diffraction analysis, and details of the analysis can be found in the Supporting Information.

Absorption and Fluorescence Spectroscopy. Ultraviolet–visible absorption spectra of solution samples are collected using a Varian Cary 50 UV/vis spectrophotometer with background correction. Tetrahydrofuran (THF, ACS, 99%+) was used as the solvent. Steady-state fluorescence spectra of solutions are collected by Spex Fluorolog Tau-3 fluorescence spectrophotometer. Peak absorbances are kept below 0.2 in order to avoid self-absorption artifacts. The samples were excited at 350 nm, and the spectra were collected from 400 to 650 nm.

Time-Resolved Fluorescence Measurements. A few drops of concentrated ethanol solution of **4F-9AC** were placed on a glass coverslip. After evaporation of the ethanol, a thin polycrystalline film of **4F-9AC** was left on the coverslip. Other samples were prepared using the same procedure. Time-resolved fluorescence lifetime data were collected using a Hamamatsu C4334 Streakscope. The solid samples were kept under a vacuum in a Janis ST100 cryostat and excited using front-face geometry. The excitation source was a 200 fs pulse centered at 387 nm, derived from frequency doubling the 775 nm output of a Spectra Physics MaiTai Ti:sapphire oscillator. The laser repetition rate was decreased to 1 MHz using a pulse picker to avoid thermal effects.

Preparation of Crystalline Microribbons and Microneedles. All the microcrystals were prepared using the floating drop method.³⁰ A total of 2.1 mg of **4F-9AC** was first dissolved in 1.0 mL of filtered ethyl acetate (Sigma, 99.5+%), and then this solution was slowly added

on top of Milli-Q Millipore purified H₂O in a Petri dish (VWR, 60 × 15 mm). The bilayer solution was covered and left undisturbed in the dark for 48 h. As the ethyl acetate evaporated, 4F-9AC slowly crystallized out as ribbons and needles floating on top of the water surface. Other microcrystals were prepared using the same procedure. The fluoro-9-anthracene carboxylic acids formed a majority of crystalline needles, in contrast to 9AC.

Optical Microscopy Measurements. To prepare samples, a few drops of 50% H₃PO₄ were added to water containing suspended microcrystals in order to slow down H₂O evaporation during the measurements. A drop of the suspension was transferred to a microscope slide and covered with a microscope coverslip. To monitor the photomechanical motion, videos were taken using a digital camera AMScope MU900 (resolution 9 M pixels). The crystals were irradiated by 405 nm light for a few seconds and then allowed to recover in the dark.

Fluorescence Recovery Measurements. A few drops of concentrated ethanol solution of the compound were placed on a glass coverslip. After evaporation of the ethanol, a thin polycrystalline film was left on the coverslip. To measure the photorecovery process, the polycrystalline film was irradiated by a 325 nm He–Cd laser for 8–18 s to photo bleach the samples around 50%. The laser power was then attenuated by a factor of 1000 or more using neutral density filters that were applied to prevent further photochemistry. The 3.1 ND filters were used for 9AC, 4F-9AC, and 2F-9AC, while the 3.6 ND filters were used for 10F-9AC and 2,6DF-9AC. This still allowed the fluorescence signal of the surviving monomer molecules to be detected to monitor the back reaction. The signals were read out by a lock-in amplifier and collected using a LabView computer program.

Nanoindentation Measurements. Nanomechanical testing was performed using a TI-950 Nanoindenter (Hysitron Minneapolis, MN), equipped with a conical indenter tip with a 1 μm radius. Two partial unload–displacement controlled indents were performed per sample at 20 different depths ranging from 20 to 450 nm. From these indentation events values of hardness, *H*, were determined using the relation³¹

$$H = \frac{P}{A} \quad (1)$$

where *P* is the maximum applied load and *A* is the area of contact. Values of the reduced elastic modulus, *E_r*, were obtained using³¹

$$E_r = \frac{\sqrt{\pi} S}{2 \sqrt{A}} \quad (2)$$

where *S* is the measured stiffness of the material upon unloading of the indenter.

RESULTS AND DISCUSSION

The synthesis of 4F-9AC, 2F-9AC, and 2,6-DF-9AC has not been previously reported. The structures of these compounds were confirmed by ¹H NMR, IR, and single crystal X-ray. All compounds were obtained in decent yields with high (>98%) purities as determined by ¹H NMR. The growth of crystals suitable for XRD measurements was somewhat challenging. Successful deposition of XRD worthy 4F-9AC and 2,6DF-9AC crystals was achieved via slow sublimation at 180 °C under normal pressure. Growing crystals of 2F-9AC was challenging due to decarboxylation at elevated temperatures, leading to crystals of 2F-9AC doped 2-fluoro-anthracene, unsuitable for XRD. Suitable crystals of 2F-9AC were slowly grown at 150 °C under reduced pressure over a period of 5 days. We found that the crystal structures of the molecules in Figure 1 are remarkably similar. In Figure 2 we show representative views of the crystal packing for the five compounds that are the subject of this paper. The crystal parameters are summarized in Table 1. From Figure 2, we can see that all four compounds crystallize in a π-stacked arrangement. The COOH groups are

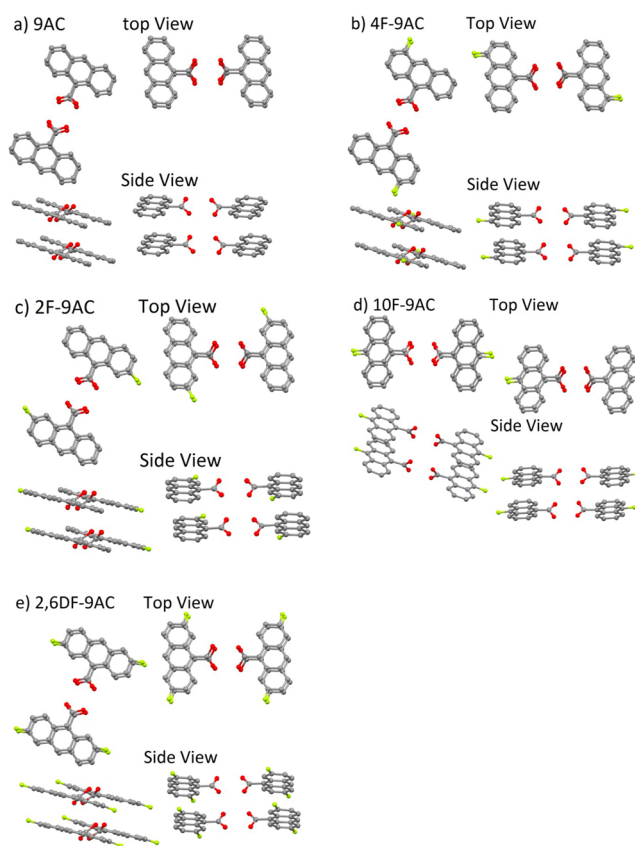


Figure 2. Top and side views of crystal structures of fluorinated anthracene-9-carboxylic acid derivatives: (a) 9AC; (b) 4F-9AC; (c) 2F-9AC; (d) 10F-9AC; and (e) 2,6DF-9AC.

all aligned to one side of the stack, which facilitates hydrogen bonding between neighboring stacks. It is this interaction that forces the 9AC derivatives to adopt the head-to-head stack motif, in contrast to the head-to-tail motif seen in crystals of most 9-substituted anthracene derivatives. The steric interference of the two COOH groups after [4 + 4] photodimer formation is believed to be the dominant factor in destabilizing the dimer and leads to the reversible photochemistry of the 9AC crystal.¹⁷ All four crystals share this packing motif with 9AC, and thus we expect all four compounds to exhibit reversible photochemistry in the crystal form, like 9AC.

Given the similarity of the crystal structures, it is not surprising that the photophysical properties of the different crystals are similar. The addition of a fluorine atom to an anthracene generally has only a small effect on the anthracene's spectroscopic properties.^{32,33} In dilute solution, the steady-state absorption spectra of all five compounds exhibit similar vibronic peak structures in their absorption spectra, resembling unsubstituted anthracene (Supporting Information, Figure S1). They also show the broad emission spectrum characteristic of anthracene carbonyl compounds, which results from a partial charge transfer from the ring to the oxygen atoms on the COOH group.³⁴ The only noticeable change is a slight redshift in the fluorinated compounds that arises from an inductive effect from the extra electrons of the substituent atoms. As expected, this redshift is most pronounced for 2,6DF-9AC. The fluorescence lifetimes of the molecules in solution (Table 2) are also similar, averaging 16 ns. The exception is 10F-9AC, whose lifetime of 5.7 ns is shorter than the other fluorinated derivatives. In solution, it does not appear that fluorine

Table 1. Crystal Parameters and X-ray Structure Refinement Parameters for 2-Fluoro-9-anthracene Carboxylic Acid (2F-9AC), 4-Fluoro-9-anthracene Carboxylic Acid (4F-9AC), and 2,6-Difluoro-9-anthracene Carboxylic Acid (2,6DF-9AC), the New Molecules Synthesized in This Work

	2F-9AC	4F-9AC	2,6DF-9AC
empirical formula	C ₁₅ H ₉ FO ₂	C ₁₅ H _{9,21} FO ₂	C ₁₅ H ₈ F ₂ O ₂
formula weight	240.22	240.44	258.21
temperature	100(2) K	100(2) K	100(2) K
wavelength	0.71073 Å	0.71073 Å	0.71073 Å
crystal system	monoclinic	monoclinic	monoclinic
space group	P2(1)/n (No. 14)	P2(1)/n (No. 14)	P2(1)/n (No. 14)
unit cell dimensions	$a = 3.7695(7)$ Å, $b = 9.4431(18)$ Å, $c = 29.486(6)$ Å, $\alpha = 90^\circ$, $\beta = 90.018(3)^\circ$, $\gamma = 90^\circ$	$a = 3.7914(4)$ Å, $b = 9.5647(10)$ Å, $c = 28.905(3)$ Å, $\alpha = 90^\circ$, $\beta = 90.472(2)^\circ$, $\gamma = 90^\circ$	$a = 3.7404(2)$ Å, $b = 9.9250(7)$ Å, $c = 29.0381(19)$ Å, $\alpha = 90^\circ$, $\beta = 90.211(1)^\circ$, $\gamma = 90^\circ$
volume	1049.6(3) Å ³	1048.15(19) Å ³	1077.99(12) Å ³
Z	4	4	4
density (calculated)	1.520 Mg/m ³	1.524 Mg/m ³	1.591 Mg/m ³
absorption coefficient	0.112 mm ⁻¹	0.112 mm ⁻¹	0.128 mm ⁻¹
F(000)	496	497	528
crystal size	0.47 × 0.30 × 0.02 mm ³	0.54 × 0.05 × 0.04 mm ³	0.33 × 0.06 × 0.02 mm ³
theta range for data collection	2.07 to 30.03°	1.41 to 27.10°	2.05 to 29.57°
index ranges	$-5 \leq h \leq 5$, $-13 \leq k \leq 13$, $-41 \leq l \leq 41$	$-4 \leq h \leq 4$, $-12 \leq k \leq 12$, $-37 \leq l \leq 37$	$-5 \leq h \leq 5$, $-13 \leq k \leq 13$, $-40 \leq l \leq 40$
reflections collected	22215	22651	24006
independent reflections	3076 [R(int) = 0.0928]	2300 [R(int) = 0.0742]	3016 [R(int) = 0.0403]
completeness to $\theta = 30.03^\circ$	99.90%	100.00%	99.90%
absorption correction	semiempirical from equivalents	semiempirical from equivalents	semiempirical from equivalents
max and min transmission	0.9981 and 0.9494	0.9960 and 0.9413	0.9974 and 0.9593
refinement method	full-matrix least-squares on F ²	full-matrix least-squares on F ²	full-matrix least-squares on F ²
data/restraints/parameters	3076/0/177	2300/588/236	3016/0/196
goodness-of-fit on F ²	1.094	1.047	1.067
final R indices [I > 2σ(I)]	R ₁ = 0.0653, wR ₂ = 0.1405	R ₁ = 0.0542, wR ₂ = 0.1399	R ₁ = 0.0488, wR ₂ = 0.1240
R indices (all data)	R ₁ = 0.0755, wR ₂ = 0.1445	R ₁ = 0.0693, wR ₂ = 0.1494	R ₁ = 0.0621, wR ₂ = 0.1324
largest diff. peak and hole	0.337 and -0.285 e-Å ⁻³	0.372 and -0.302 e-Å ⁻³	0.327 and -0.248 e-Å ⁻³

Table 2. Fluorescence Lifetimes in the Solid-State and in Solution for 9AC, 2F-9AC, 4F-9AC, 10F-9AC, and 2,6DF-9AC^a

	τ_1 (ns)	τ_2 (ns)	A_1	A_2	solution τ_s (ns)
9AC	6.0 ± 0.4	33.0 ± 0.5	0.31	0.69	15.3 ± 0.1
2F-9AC	3.1 ± 0.2	24.0 ± 0.3	0.42	0.58	18.0 ± 0.1
4F-9AC	1.8 ± 0.1	21.7 ± 0.1	0.15	0.85	17.2 ± 0.2
10F-9AC	3.2 ± 0.1	10.7 ± 0.1	0.50	0.50	5.7 ± 0.5
2,6DF-9AC	3.8 ± 0.2	18.1 ± 0.6	0.66	0.34	15.6 ± 0.2

^aThe solid state fluorescence lifetime decay was fit to a biexponential decay of the form $A_1 \exp[t/\tau_1] + A_2 \exp[t/\tau_2]$. The solution lifetime decay was fit to a single exponential decay of the form $A \exp[t/\tau_s]$.

substitution has a dramatic effect on the molecular electronic state structure and dynamics. The solid-state fluorescence and excitation spectra are shown in Figure 3. Again, the different compounds show similar broadened excitation and emission spectra. The solid-state fluorescence line shape is characteristic of excimer formation, as expected for the π -stacked crystal. The

solid-state fluorescence decays are biexponential in general, with a short component on the order of 3 ns and a longer-lived component on the order of 20–30 ns (Table 2). The exception once again is 10F-9AC, whose long-time decay component is significantly shorter at 10.7 ns. The nonexponential decays of the 9AC derivatives indicates that the structural disorder inferred from the XRD data leads to a distribution of relaxation times and possibly reaction rates.

Given the structural and spectroscopic similarities of the five compounds, we had little reason to expect dramatically different photomechanical properties. We began by measuring the lifetime of the metastable photodimer in different crystals. To accomplish this, we utilized a fluorescence recovery experiment. In this experiment, a brief pulse of 325 nm laser light reacts a fraction of the monomer, typically about 50%. The laser is then attenuated to a level where the photochemistry is negligible but the fluorescence signal from the surviving monomer molecules can still be detected. The dimer photoproduct has negligible absorption at 325 nm and does not contribute to the fluorescence signal. As the photodimer dissociates back into

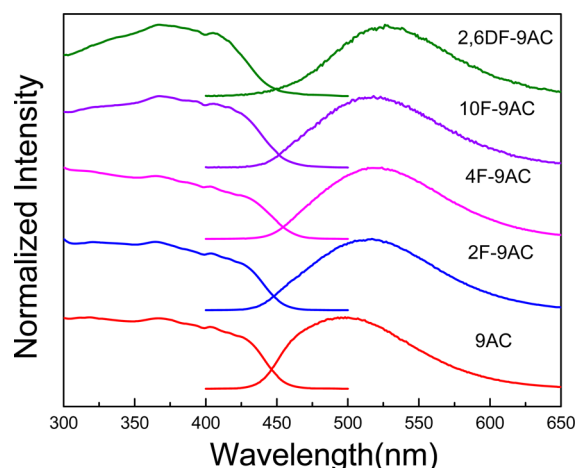


Figure 3. Solid-state excitation and emission spectra of anthracene-9-carboxylic acid (9AC) and its fluorinated derivatives: (a) 9AC; (b) 2F-9AC; (c) 4F-9AC; (d) 10F-9AC, and (e) 2,6DF-9AC. The solid line plots are the excitation spectra, and the dotted line plots are the emission spectra. For the emission spectra, samples were excited at 350 nm. Solution spectra are given in the Supporting Information (Figure S1).

monomers, the fluorescence signal recovers to an asymptotic value. Ideally, this value is identical to the fluorescence signal before the light pulse, but in most cases it is slightly (10–20%) below that value due to crystal movement or photobleaching. Typical data traces are shown in Figure 4 for 4F-9AC, 2F-9AC,

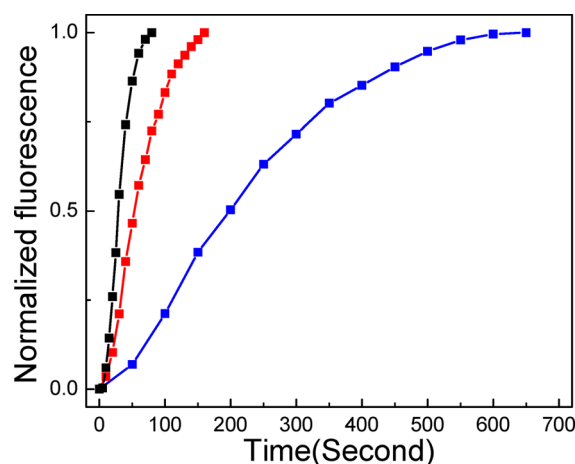


Figure 4. Fluorescence recovery curves of 4F-9AC (black), 2F-9AC (red), and 9AC (blue). Prior to the probing of the photorecovery, all three crystalline films were photoreacted by ~50%. For comparison, the residual signal after photoreaction was subtracted from the data, and the recovery curves were normalized so they recovered to an asymptotic value of 1. In the experiment, 9AC and 2F-9AC crystals recovered to 70–80% of their original signals, while 4F-9AC crystals recovered to 94% of its original signal. The fluorescence recovery data of 2,6DF-9AC and 10F-9AC crystals are given in the Supporting Information, Figure S3.

and 9AC. It is clear that the recovery rates are very different in these three crystals. It is also clear that the recovery is nonexponential, from the time-lag in the growth at early times. This nonexponential behavior is a symptom of nucleation kinetics, which has been observed in the solid-state dimerization of 9AC.³⁵ Rather than try to quantitatively

model the kinetics, we simply define $\tau_{1/2}$ as the time required for the fluorescence to attain 50% of its asymptotic value. Table 3 gives the average $\tau_{1/2}$ values for the different compounds

Table 3. Fluorescence Recovery Half Time ($\tau_{1/2}$) of 9AC and Its Fluorinated Derivatives

	$\tau_{1/2}$ (s)
9AC	200 ± 20
2F-9AC	55 ± 5
4F-9AC	25 ± 3
10F-9AC	400 ± 40
2,6DF-9AC	60 ± 6

shown in Figure 1. 4F-9AC undergoes a fluorescence recovery that is almost 10 times more rapid than that of 9AC, while 10F-9AC is significantly slower than 9AC. 2F-9AC and 2,6DF-9AC were considerably more rapid than 9AC but still a factor of 2 slower than 4F-9AC. The large variation in recovery times was unexpected given the similarity of crystal structures and spectroscopic properties of these compounds.

An important question is whether the mechanical recovery mirrors the fluorescence recovery. We recently analyzed the connection between reaction progress and mechanical deformation for the solid-state [4 + 4] photodimerization of 9-methylantracene, showing that the mechanical response mirrors the reaction progress but with a slight time lag.³⁶ We have also shown that 9AC nanorod bending closely follows the photochemical reaction progress.¹⁹ Even though 4F-9AC is a different molecule, we expect a similar dynamical picture to hold for it as well, with the mechanical response time of 4F-9AC being ~10× faster than that of 9AC. In Figure 5 we

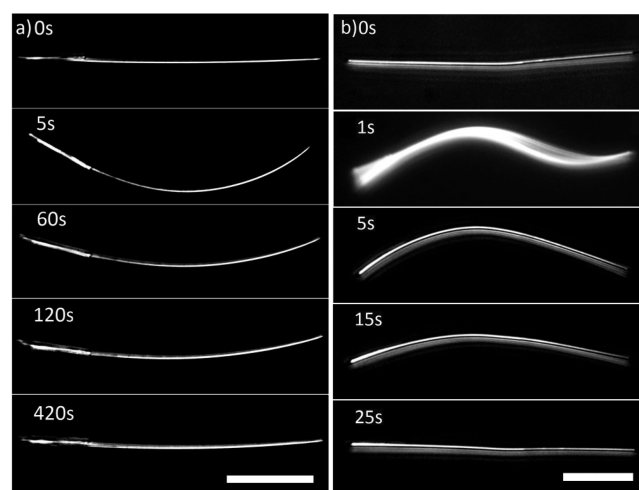


Figure 5. Series of optical microscopy images of (a) 9AC and (b) 4F-9AC. The 4F-9AC crystal completely untwists in 25 s, while the 9AC crystal requires 420 s to unbend. Both scale bars are 50 μm .

compare a series of images for microribbons composed of 9AC and 4F-9AC after irradiation causes them to twist. The 4F-9AC ribbon completely untwists within 30 s, while the 9AC ribbon requires ~400 s. Thus, the mechanical recovery rate closely tracks the fluorescence recovery rate, as expected. We find that, for all the compounds, given comparable crystals, the mechanical recovery times parallel the fluorescence recovery times. Quantitative comparison of the mechanical recovery times is difficult due to the fact that different crystals have

different shapes and degrees of adhesion to the substrate, leading to variations in the observed recovery times. Typically, 4F-9AC shows the most rapid mechanical recovery, with 2F-9AC slower by a factor of ~ 2 , 9AC slower by a factor of ~ 10 , and 10F-9AC slower by a factor of ~ 25 . We found it difficult to obtain consistent results for the mechanical recovery of 2,6DF-9AC, since it often did not recover its original shape, despite the fact that the fluorescence recovered. In order to compare absolute mechanical recovery times between different molecular crystals, we would need uniform samples where all the crystals are the same size and shape. In this paper only the qualitative correlations as shown in Figure 5 are presented.

In addition to their faster recovery time, 4F-9AC crystals were more resistant to cracking and fracture than 9AC crystals. In Figure 6, two similarly sized, large ($>20 \mu\text{m}$) crystals of 9AC

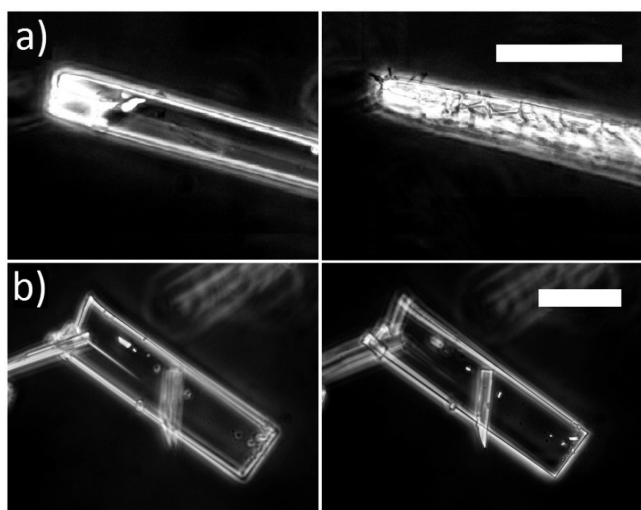


Figure 6. Optical microscopy images of 9AC and 4F-9AC crystals. (a) 9AC crystal before and after irradiation. The 9AC crystal shatters into pieces after irradiation. (b) 4F-9AC before and after irradiation. After irradiation, the 4F-9AC crystal stays intact. Both scale bars are $50 \mu\text{m}$.

and 4F-9AC are shown before and after irradiation at 405 nm for 5 s. These crystals are too large to exhibit the bending and twisting seen in smaller needles and ribbons.³⁷ The 9AC crystal loses many surface fragments during exposure and obviously never recovers its original morphology, while the 4F-9AC crystal stays intact and does not fragment. This appears to be a general property of the 4F-9AC crystals. Even relatively large crystals could survive irradiation conditions that would cause similar 9AC crystals to disintegrate. This improved robustness was previously observed for 10F-9AC crystals as well.²⁴ In order to investigate the physical origin of this effect, the mechanical properties of the monomer crystals were measured using a nanoindentation method.^{31,38} The measured reduced elastic modulus and hardness for 9AC were determined to be 9.58 and 0.46 GPa, respectively, while the reduced elastic modulus and hardness of 4F-9AC were 6.98 and 0.27 GPa, respectively (Supporting Information, Figure S4). Post-indentation optical analysis of 9AC revealed that the material was fractured. The E_r values are typical for organic molecular crystals. Both the reduced elastic modulus and hardness of 4F-9AC are less than 9AC, but the hardness decreases more than the elastic modulus. The tendency of a material to develop cracks is proportional to the ratio of hardness to elastic modulus,^{39,40} which is 0.0486 for 9AC and 0.0392 for 4F-9AC.

The more brittle nature of 9AC compared to 4F-9AC can be attributed to the greater hardness of 9AC, and thus we expect this crystal to crack more readily in response to the internal strain generated by the photodimerization. This is consistent with our observations, suggesting that mechanical measurements of the reactant crystal may provide useful parameters for evaluating photomechanical molecular crystals.

In addition to being less prone to fragmentation, 4F-9AC crystals also show improved mechanical cycling behavior. It was previously found that 9AC nanorods and microribbons could be repeatedly bent or twisted, but only for a limited number of cycles, typically less than 10^{18} . In contrast, ribbons and needles composed of 4F-9AC could undergo 100 or more photo-mechanical cycles without noticeable loss of response. An example is shown in Figure 7, where a 4F-9AC microneedle bends under the repeated application of 405 nm light. The crystal shows complete motion and full recovery even after 115 cycles. Additional images of repeated microribbon twisting can be found in the Supporting Information (Figure S5). This

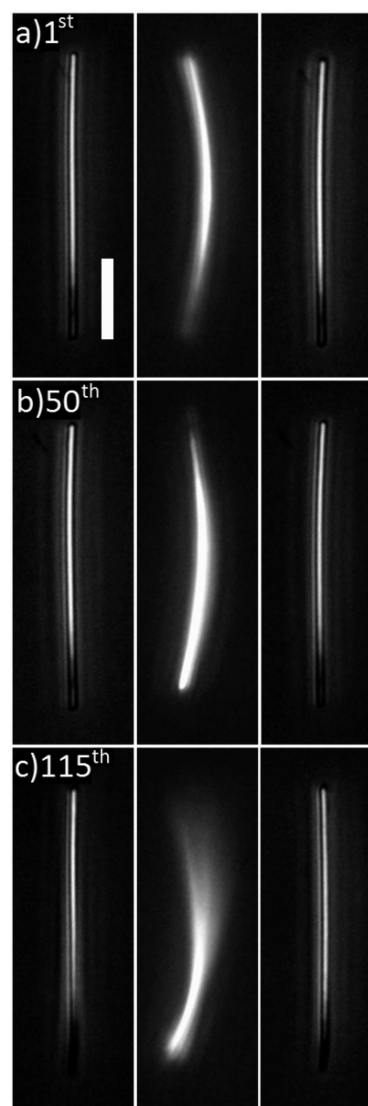


Figure 7. Snapshots of repeated cycles of 4F-9AC crystalline needle's photoinduced bending and recovery: (a) 1st cycle; (b) 50th cycle; and (c) 115th cycle. The irradiation source was a 100 W Hg lamp. Scale bar is $20 \mu\text{m}$.

enhanced robustness puts this group of molecules in the same class as the fluorinated diarylethenes.^{13,14} The intermolecular anthracene [4 + 4] dimerization reaction, however, is much more disruptive than the intramolecular diarylethene ring opening–closing reaction in the sense that it involves larger nuclear displacements by more atoms. Given this, the fact that the 4F-9AC crystals remain intact and responsive after multiple reaction cycles is remarkable. The fluorinated anthracene is expected to be more stable with respect to photochemical oxidation side reactions.⁴¹ What is perhaps more surprising is that crystal defect formation and fracture do not seem to be major degradation pathways in this crystal. For the latter effect, the reduced hardness of the 4F-9AC crystal may be an important factor that affects degradation.

The results described above demonstrate that the photo-mechanical behavior of the 4F-9AC crystal represents a significant improvement over that of 9AC, but the physical origin of this improved behavior is not clear. Fluorine substitution has been used as a strategy for changing crystal packing to enhance photochemical reactivity.^{42,43} But as discussed above, all five compounds have very similar crystal packing geometries and photophysical properties. It should be noted, however, that the crystals have varying amounts of disorder and some variations in twinning behavior and impurity levels. One concern is that the different mechanical behaviors could be due to differences in crystal quality between the different molecules. But defects and impurities would not be expected to change the dimer dissociation rates, which result from very localized molecular interactions. The fact that the different mechanical response rates mirror the fluorescence recovery rates suggests that the changes in the mechanical properties are due to changes in the intrinsic crystal structure, as opposed to differences in crystal quality.

If we assume that the changes in behavior are due to intrinsic crystal properties, then the fluorine atoms must be the key. Organic fluorine substitution can lead to multiple different hydrogen and halogen bonding interactions which have the potential to modify material properties.⁴⁴ We suspect that the faster dimer dissociation and increased plasticity of the 4F-9AC crystals both stem from changing noncovalent interactions in the crystal. There are several possible culprits. Fluorine substitution can affect π – π interactions due to the electron-withdrawing effects of the F atoms, leading to enhanced photodimerization. However, the small change in the interplanar distances (Table 4) and the similarity in crystal packing suggests that this effect is not large. Noncovalent bonding interactions, for example H...F interactions, can stabilize crystal structures. If we assume that these bonds are broken when the photodimer is formed, then the stabilization energy of the H...F interactions would provide an extra driving

Table 4. Distances between Two Adjacent π – π Stacked Molecules of 9AC, 2F-9AC, 4F-9AC, 10F-9AC, and 2,6DF-9AC

	$D_{\pi-\pi}$ (Å)
9AC	3.473 ^a
2F-9AC	3.438
4F-9AC	3.446
10F-9AC	3.436 ^b
2,6DF-9AC	3.412

^aData taken from ref 45. ^bData taken from ref 24.

force for the dissociation reaction and lead to more rapid recovery. The photodimer dissociation would be driven partly by the energetic gain derived from reestablishing the hydrogen bond network. Determining which molecule has the strongest hydrogen bonding interactions from the crystal structures in Figure 2 is not easy, especially given the disorder in the crystal structures. In order to assess how intermolecular forces affect the energetics of the monomer–dimer reaction, we are collaborating with a theoretical group. Ideally, we would be able to correlate the relative stability of the photodimers with the observed recovery rate. Although the microscopic origins of the different behaviors are currently unclear, the observation that large changes in the photomechanical performance of the crystals can be achieved by small changes in the constituent molecular structure represents the most important conclusion of this paper.

CONCLUSIONS

We have synthesized and characterized four fluorinated derivatives of 9AC, a molecule that shows a reversible photomechanical response in its crystal form. These new molecules have similar molecular electronic structure and dynamics, as well as similar crystal packing motifs, but different photomechanical properties. One of these derivatives, 4F-9AC, exhibits an order of magnitude improvement in both its recovery time and its cycling ability relative to 9AC. It appears that subtle interactions arising from changes in the π – π interactions or hydrogen bonding between molecules are responsible for the changes in the crystal photomechanical properties. An improved understanding of these interactions will require the help of computational chemistry to quantify energetic differences between the different crystals. The results in this paper demonstrate that it is possible to significantly improve the properties of photomechanical materials based on the anthracene [4 + 4] photodimerization reaction through molecular engineering. It is likely that advances in both organic synthesis and crystal engineering will lead to dynamic molecular crystals with improved performance.

ASSOCIATED CONTENT

Supporting Information

¹H-NMR of 4F-9AC and synthesis of fluoro–anthracene carboxylic acids; spectroscopic properties of fluoro–anthracene carboxylic acids; photomechanical properties of 9AC and 4F-9AC; and crystallographic information for 2F-9AC, 4F-9AC, 2,6DF-9AC, and 10F-9AC. This material is available free of charge via the Internet at <http://pubs.acs.org>.

AUTHOR INFORMATION

Corresponding Authors

*E-mail: christopher.bardeen@ucr.edu (C.J.B).

*E-mail: kaysir@ksau-hs.edu.sa; rabihalkaysi@gmail.com (R.O.K.).

Notes

The authors declare no competing financial interest.

ACKNOWLEDGMENTS

This research was supported by the National Science Foundation Grant DMR-1207063 (C.J.B.), by the Air Force Office of Scientific Research Grant FA9550-12-1-0245 (D.K.), and by the King Abdulaziz City for Science and Technology (KACST) Grant AT-30-435 (R.O.K.).

■ REFERENCES

- (1) Kim, T.; Zhu, L.; Al-Kaysi, R. O.; Bardeen, C. J. *ChemPhysChem* **2014**, *15*, 400–414.
- (2) Finkelmann, H.; Nishikawa, E.; Pereira, G. G.; Warner, M. *Phys. Rev. Lett.* **2001**, *87*, 015501/1–015501/4.
- (3) Ikeda, T.; Mamiya, J.; Yu, Y. *Angew. Chem., Int. Ed.* **2007**, *46*, 506–528.
- (4) Barrett, C. J.; Mamiya, J.; Yager, K. G.; Ikeda, T. *Soft Matter* **2007**, *3*, 1249–1261.
- (5) Lange, C. W.; Foldeaki, M.; Nevodchikov, V. I.; Cherkasov, V. K.; Abakumov, G. A.; Pierpont, C. G. *J. Am. Chem. Soc.* **1992**, *114*, 4220–4222.
- (6) Koshima, H.; Nakaya, H.; Uchimoto, H.; Ojima, N. *Chem. Lett.* **2012**, *41*, 107–109.
- (7) Koshima, H.; Takechi, K.; Uchimoto, H.; Shiro, M.; Hashizume, D. *Chem. Commun.* **2011**, *47*, 11423–11425.
- (8) Naumov, P.; Sahoo, S. C.; Zakharov, B. Z.; Boldyreva, E. V. *Angew. Chem., Int. Ed.* **2013**, *52*, 9990–9995.
- (9) Bushuyev, O. S.; Tomberg, A.; Friscic, T.; Barrett, C. J. *J. Am. Chem. Soc.* **2013**, *135*, 12556–12559.
- (10) Nath, N. N.; Pejov, L.; Nichols, S. M.; Hu, C.; Saleh, N.; Kahr, B.; Naumov, P. *J. Am. Chem. Soc.* **2014**, *136*, 2757–2766.
- (11) Irie, M.; Yokoyama, Y.; Seki, T. *New Frontiers in Photochromism*; Springer: Japan, 2013.
- (12) Roberts, R. J.; Rowe, R. C.; York, P. *Powder Technol.* **1991**, *65*, 139–146.
- (13) Kobatake, S.; Takami, S.; Muto, H.; Ishikawa, T.; Irie, M. *Nature* **2007**, *446*, 778–781.
- (14) Morimoto, M.; Irie, M. *J. Am. Chem. Soc.* **2010**, *132*, 14172–14178.
- (15) Terao, F.; Morimoto, M.; Irie, M. *Angew. Chem., Int. Ed.* **2012**, *51*, 901–904.
- (16) Irie, M. *Chem. Rev.* **2000**, *100*, 1685–1716.
- (17) Ito, Y.; Fujita, H. *J. Org. Chem.* **1996**, *61*, 5677–5680.
- (18) Al-Kaysi, R. O.; Bardeen, C. J. *Adv. Mater.* **2007**, *19*, 1276–1280.
- (19) Good, J. T.; Burdett, J. J.; Bardeen, C. J. *Small* **2009**, *5*, 2902–2909.
- (20) Zhu, L.; Al-Kaysi, R. O.; Bardeen, C. J. *J. Am. Chem. Soc.* **2011**, *133*, 12569–12575.
- (21) Takahashi, S.; Miura, H.; Kasai, H.; Okada, S.; Oikawa, H.; Nakanishi, H. *J. Am. Chem. Soc.* **2002**, *124*, 10944–10945.
- (22) Al-Kaysi, R. O.; Muller, A. M.; Bardeen, C. J. *J. Am. Chem. Soc.* **2006**, *128*, 15938–15939.
- (23) Bucar, D. K.; MacGillivray, L. R. *J. Am. Chem. Soc.* **2007**, *129*, 32–33.
- (24) Zhu, L.; Al-Kaysi, R. O.; Dillon, R. J.; Tham, F. S.; Bardeen, C. J. *Cryst. Growth Des.* **2011**, *11*, 4975–4983.
- (25) Kaur, I.; Jia, W.; Kopreski, R. P.; Selvarasah, S.; Dokmeci, M. R.; Pramanik, C.; McGruer, N. E.; Miller, G. P. *J. Am. Chem. Soc.* **2008**, *130*, 16274–16286.
- (26) Rochlin, E.; Rappaport, Z. *J. Org. Chem.* **2003**, *68*, 216–226.
- (27) Yakamoto, G.; Suzuki, M.; Oki, M. *Bull. Chem. Soc. Jpn.* **1983**, *56*, 306–313.
- (28) Bergmann, E. D.; Berkovic, S. *J. Org. Chem.* **1961**, *26*, 919–923.
- (29) Dewar, M. J. S.; Michl, J. *Tetrahedron* **1970**, *26*, 375–384.
- (30) Campione, M.; Ruggerone, R.; Tavazzi, S.; Moret, M. *J. Mater. Chem.* **2005**, *15*, 2437–2443.
- (31) Oliver, W. C.; Pharr, G. M. *J. Mater. Res.* **2004**, *19*, 3–20.
- (32) Medina, B. M.; Beljonne, D.; Egelhaaf, H. J.; Gierschner, J. *J. Chem. Phys.* **2007**, *126*, 111101/1–111101/6.
- (33) Tannaci, J. F.; Noji, M.; McBee, J.; Tilley, T. D. *J. Org. Chem.* **2007**, *72*, 5567–5573.
- (34) Dey, J.; Haynes, J. L.; Warner, I. M.; Chandra, A. K. *J. Phys. Chem. A* **1997**, *101*, 2271–2278.
- (35) More, R.; Busse, G.; Hallmann, J.; Paulmann, C.; Scholz, M.; Teichert, S. *J. Phys. Chem. C* **2010**, *114*, 4142–4148.
- (36) Kim, T.; Zhu, L.; Mueller, L. J.; Bardeen, C. J. *J. Am. Chem. Soc.* **2014**, *136*, 6617–6625.
- (37) Kim, T.; Zhu, L.; Mueller, L. J.; Bardeen, C. J. *CrystEngComm* **2012**, *14*, 7792–7799.
- (38) Varughese, S.; Kiran, M. S. R. N.; Ramamurty, U.; Desiraju, G. R. *Angew. Chem., Int. Ed.* **2013**, *52*, 2701–2712.
- (39) Lawn, B. R.; Evans, A. G.; Marshall, D. B. *J. Am. Ceram. Soc.* **1980**, *63*, 574–581.
- (40) Lawn, B. R.; Marshall, D. B. *J. Am. Ceram. Soc.* **1979**, *62*, 347–350.
- (41) Matsubara, Y.; Kimura, A.; Yamaguchi, Y.; Yoshida, Z. *Org. Lett.* **2008**, *10*, 5541–5544.
- (42) Kumar, V. A.; Begum, N. S.; Venkatesan, K. *J. Chem. Soc., Perkin Trans. 2* **1993**, 463–467.
- (43) Sonoda, Y. *Molecules* **2011**, *16*, 119–148.
- (44) Berger, R.; Resnati, G.; Metrangolo, P.; Weber, E.; Hulliger, J. *Chem. Soc. Rev.* **2011**, *40*, 3496–3508.
- (45) More, R.; Scholz, M.; Busse, G.; Busse, L.; Paulmann, C.; Tolkiehn, M.; Teichert, S. *Phys. Chem. Chem. Phys.* **2012**, *14*, 10187–10195.